Carbon 222 (2024) 118952

Contents lists available at ScienceDirect

Carbon

journal homepage: www.elsevier.com/locate/carbon

Research paper

Behavior of localized states in double twisted ABC trilayer graphene

Felipe Pérez Riffo [a], Sanber Vizcaya [a], E. Menéndez-Proupin [b], Juan M. Florez [a], Leonor Chico [c], Eric Suárez Morell [a,b,*]

[a] Grupo de Simulaciones, Departamento de Física, Universidad Técnica Federico Santa María, Casilla 110-V, Valparaíso, Chile
[b] Departamento de Física Aplicada I, Escuela Politécnica Superior, Universidad de Sevilla, Seville, E-41011, Spain
[c] GISC, Departamento de Física de Materiales, Facultad de Ciencias Físicas, Universidad Complutense de Madrid, 28040 Madrid, Spain

ARTICLE INFO

Keywords:
Graphene
Trilayers
Twistronic
Localized states

ABSTRACT

We show that a double-twisted ABC trilayer graphene, formed by stacking two ABC trilayers with a rotation angle between them, is a semiconductor with a gap of about 30 meV. Importantly, flat bands in the electronic structure are observed even for large angles, and the localization of electrons follows the same pattern as in ABC trilayer graphene. Our first-principles calculations show that this behavior holds at least for rotation angles from 7 to 21 degrees. We further study the charge redistribution as a function of the angle. Below two degrees, the charge escapes from the rotated layers and AA zones, moving to the outer layers. This behavior is general for any ABA trilayer with one of the outer layers twisted (ABT). Our findings shed light on some peculiarities of rotated graphene, explaining the absence of a superconductivity phase on these double-trilayer and ABT systems.

1. Introduction

Interlayer rotation has become a ubiquitous tool for studying and tuning the properties of coupled atomic monolayers. The modification of the electronic properties of bilayer systems, sometimes dramatically, has been theoretically explored since more than a decade [1–6], but the discovery of superconductivity in twisted bilayer graphene (TBG) [7] has resulted in thousands of investigations delving into the possible mechanisms giving rise to this phenomenon. Superconductivity has also been found in graphene trilayers [8] and tetralayers [9] and has been suggested to occur in quasi-one-dimensional systems such as collapsed graphene nanotubes [10,11]. As a matter of fact, changing the stacking between layers can also produce structures with different properties in these multilayer systems. Specifically, there are two stable stacks with three graphene layers: ABA (Bernal) and ABC (rhombohedral). In the Bernal stacking, the bands near the Fermi level have a monolayer and bilayer-like character, with linear and quadratic dispersions, respectively [12–14]. When an external electric field is applied perpendicularly to the layers, the bands hybridize and overlap without a gap. In contrast, in the ABC stacking (see Fig. 1a), the low-energy bands have a cubic dispersion (Fig. 1b dashed lines), with flat bands near the Fermi level [15]. The high density of states associated with this behavior indicates that interactions could be crucial. In this case, the symmetry group is D_{3d}, and the system has inversion symmetry. Therefore, a gap between the conduction and valence bands can be opened with an external electric field [15–19], and it can be tunable [20,21]. Indeed, if the external field is small (a few meV) van Hove singularities appear near the Fermi level (Fig. 1b solid line). Doping the system to reach those states leads to collective behavior as ferromagnetism [22] and superconductivity [23].

Recent experiments prove [24] that by placing an ABC trilayer aligned on an hBN monolayer, the moiré potential induces flat minibands that exhibit Mott insulating behavior at certain band fillings. Additionally, without screening by the substrate, a suspended ABC trilayer opens a gap spontaneously, apparently due to electron–electron interaction. The system would have electrons with opposite spins in the valence and conduction bands closer to the Fermi level [25]. For more information on collective phenomena in unrotated structures, the reader is encouraged to consult Ref. [26].

In addition to the well-known ABA and ABC stackings, it is possible to obtain other properties in three-layer structures by rotating one of the layers. Specifically, if we have one of these two stackings and rotate the third layer, we obtain a system that can be visualized as two coupled AB layers and a twisted outer layer, i.e., AB-twisted (ABT) graphene [27]. In this system, there is a gap between the parabolic bands. For small rotational angles, it can be explained as an energy upshift of the states located at the AA region and the Fermi level, creating an effective potential difference between the AB layers [27].

* Corresponding author at: Grupo de Simulaciones, Departamento de Física, Universidad Técnica Federico Santa María, Casilla 110-V, Valparaíso, Chile.
E-mail address: eric.suarez@usm.cl (E.S. Morell).

https://doi.org/10.1016/j.carbon.2024.118952
Received 13 January 2024; Received in revised form 14 February 2024; Accepted 17 February 2024
Available online 23 February 2024

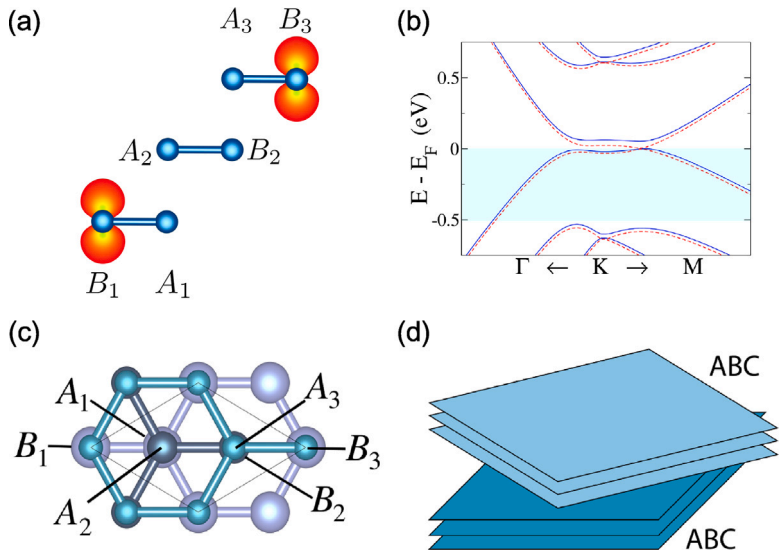

Fig. 1. (a) Localization of states in the bonding orbitals in ABC trilayer (lateral view). The states are from the shadowed region of (b), where the DFT calculation of the electronic structure of trilayer ABC is shown around the K point. Red dashed lines are the bands without external field, blue solid lines for $\mathbf{E} = 10$ meV/Å $\hat{z}$. (c) Top view of trilayer ABC. (d) Scheme of the double twisted ABC trilayer structure.

Systems with four layers show similar electronic properties. The double twisted bilayer graphene (DTBG) consists of two bilayer graphene in AB stacking, placed one on top of the other, with a rotational angle between them. DTBG presents an intrinsic gap for large angles; however, it is metallic for low angles with flat bands [28–31]. Experimental studies of this configuration found the existence of correlated states and the band gap opening by an external electric field [9,32].

This article shows that two coupled ABC trilayers with an arbitrary twist angle constitute a semiconducting system with flat bands, even for relatively large rotations, well away from the magic angle. This behavior is similar to an ABC trilayer submitted to an external bias. Using a tight-binding (TB) model, we further study how the charge redistributes within the layers as a function of angle. We find that for rotation angles smaller than two degrees the charge escapes from the rotated inner layers and AA zones and moves to the outer layers. Indeed, the same behavior occurs in any trilayer ABT system. We quantify the effect and offer a qualitative explanation of its origin. We also clarify this behavior with a toy model of a trilayer with only six atoms by adding an onsite energy term to the rotated layers. Our work throws light on why a superconducting phase in this type of structure has not been found.

This article is organized as follows: In Section 2, Methods, we explain the details of the ab-initio calculation and the tight-binding Hamiltonian used. In Section 3, Calculations, we review the ABC trilayer with emphasis on the localization of the states in the presence of a small external field. We then explain the results of the rotated double ABC, its electronic structure, and the spatial localization of the states near the Fermi level. We then dedicate a subsection to understanding the localization of these states, for which we analyze and compare to a more straightforward system with the same behavior, the ABT, a three-layer ABA system where we rotate the third layer. Finally, we summarize and discuss our results.

2. Methods

In this work, we employ a combination of density functional theory(DFT)-based models, tight-binding and molecular dynamics in order to obtain the electronic structure of six-layered twisted structures up to the magic angle.

DFT is considered a pillar of the standard model of solids [33]. Many computational packages implement DFT to compute ground state properties of solids from first principles, i.e., without empirical parameters other than the atomic coordinates. DFT has been a very successful method for systems with moderate electron correlation. Moreover, DFT calculations provide input wavefunctions for more sophisticated methods that improve the DFT accuracy, like quantum Monte Carlo (QMC) and dynamic mean field theory (DMFT), or extend its capabilities to excited states, like the GW method and the Bethe–Salpeter equation [34]. DMFT and QMC have been recently employed to study strong correlations near the magic angle for twisted bilayers [35,36]. However, for our purposes, i.e., the confinement of the charge as a necessary condition for the existence of correlated phenomena, it is sufficient to resort to DFT calculations, which is already a formidable task in a six-layered structure for small rotation angles.

2.1. Unit cell

We construct the unit cell used in the calculations performed within the DFT approach and the tight-binding (TB) method following the standard procedure [3,6]. We generate 6 layers with ABC–ABC stacking and then rotate the top three layers. The rotation axis is located at the origin, and at that point, there is one atom on top of another in layers 3 and 4, so that region is the AA zone of the commensurate unit cell. One of the lattice vectors of the moiré cell is $\mathbf{T} = n\mathbf{a}_1 + m\mathbf{a}_2$, where n and m are integers, and $\mathbf{a}_{1,2}$ are the graphene lattice vectors forming an angle of 60°. The cells studied are of type $m = n - 1$. We indistinctly label the cells with the angle or the index n. For DFT calculations, the layers are placed centered in $\hat{z}$ with the lattice vector $c = 40$ Å to guarantee a wide enough vacuum and the non-interaction between replicas [37].

The space group of two ABC twisted structures is 150 [38], like twisted bilayer graphene.

2.2. DFT calculations

The positions of the layers have been optimized by means of total energy DFT calculations with the projector augmented wave (PAW) method [39,40], as implemented in the Vienna ab initio Simulation Package (VASP) [41,42]. PAW potentials include the $1s^2$ electronic shell in the core, treating explicitly the $2s^2 3p^2$ electrons. The single electron wavefunctions are obtained from an expansion in a plane wave basis set with a cutoff of 520 eV, i.e., the basis set is truncated, restricting the largest wavevector $\mathbf{G}$ by the expression $\hbar^2 G^2/2m_0 \leq 520$ eV. The

exchange and correlation interaction is calculated with the functional of Perdew, Burke, and Ernzerhof [43]. Dispersion interaction is included by means of a Grimme DFT-D3 correction with Becke-Johnson damping function [44,45].

DFT band calculations are performed while keeping the self-consistently computed charge density constant. The atomic positions and lattice vectors were relaxed until forces were smaller than 0.01 eV/Å, and all stress tensor components were smaller than 0.5 kbar. The latter condition is achieved even for the z component despite the c vector not being optimized, thus indicating that the vacuum region set in the unit cell is wide enough. Γ-centered regular k-point grids have been used with dimensions $8 \times 8 \times 1$, $5 \times 5 \times 1$, $4 \times 4 \times 1$ and $3 \times 3 \times 1$ for $n = 2$ (21.8°), 3 (13.2°), 4 (9.4°), and 5 (7.3°) structures, respectively.

2.3. Tight-binding model and lattice relaxation

The band structure for low angles is obtained using a tight-binding model following Nam and Koshino [46]:

$$H = \sum_i \Delta_i |\mathbf{R}_i\rangle\langle\mathbf{R}_i| - \sum_{i,j} t(\mathbf{R}_i - \mathbf{R}_j)|\mathbf{R}_i\rangle\langle\mathbf{R}_j| + \text{H.c.}, \tag{1}$$

where $\mathbf{R}_i$ is the position of the atom i, $|\mathbf{R}_i\rangle$ is the wavefunction at site i, $\Delta_i = \pm 20$ meV is an onsite term that takes a positive or negative value depending on the layer. This term has to be added to address the crystal field related to a charge transfer between layers. $t(\mathbf{R})$ is the hopping between atoms i and j:

$$-t(\mathbf{R}) = V_{pp\pi}(R)\left[1 - \left(\frac{\mathbf{R}\cdot\mathbf{e}_y}{R}\right)^2\right] + V_{pp\sigma}(R)\left(\frac{\mathbf{R}\cdot\mathbf{e}_y}{R}\right)^2 \tag{2}$$

The explicit expression of the hopping parameters $V_{pp\pi}(R)$ and $V_{pp\sigma}(R)$ is:

$$V_{pp\pi}(R) = V^0_{pp\pi}\exp\left(-\frac{R-a_0}{r_0}\right) \tag{3}$$

$$V_{pp\sigma}(R) = V^0_{pp\sigma}\exp\left(-\frac{R-d_0}{r_0}\right), \tag{4}$$

with $V^0_{pp\pi} = -2.65$ eV and $V^0_{pp\sigma} = 0.48$ eV. $a_0 = a/\sqrt{3} \simeq 1.42$ Å is the nearest-neighbor distance in graphene, $d_0 = 3.35$ Å is the interlayer distance (with a being the interatomic distance), and $r_0 = 0.184\,a$ is the decay length of the interaction. We slightly modified the value of $V^0_{pp\pi}$ for a better match with DFT bands.

Although TB calculations were performed for on-site energy values that simulate the DFT results, we found that the result is robust and does not depend on these values; even for on-site values equal to zero, the same trend is obtained.

We have also investigated how atomic relaxations affect the electronic structure. Using LAMMPS [47], energy minimization was performed for non-bonded interlayer interactions using the Kolmogorov–Crespi potential [48,49] with a cutoff of 20 Å and bonded intralayer interactions using the REBO potential [50,51]. The relaxations were done with an energy tolerance of 10^{-10} eV per atom [52].

We want to emphasize that for rotated bilayer graphene, the relaxation of the structures and, thus, the reduction of the AA zones has the greatest impact precisely at small angles. If a rigid rotation is carried out, the AA zone becomes larger. When we relax the structures due to the lower energy of the AB (BA) zones, the cell is reconstructed by shrinking the AA zones. This impacts the electronic structure for angles close to the magic angle of 1.05° . For angles larger than 2°, such impact is not noticeable, in our calculations of the charge per layer, there is minimal impact on the charge distribution due to relaxation. The tendency is the same if we calculate with the rigid structure. Therefore, a relaxed structure was used for all TB calculations for angles below 2°; above that angle, the effect of the relaxation on the electronic structure is not noticeable.

3. Calculations

3.1. ABC trilayer

In Fig. 1b, we show the band structures of ABC trilayer without (blue solid line) and with a small external field of 10 meV/Å (red dashed lines). An external electric field breaks the inversion symmetry and opens a gap.

Another notable difference exists between the ABA trilayer and the ABC (rhombohedral) trilayer. The middle layer in ABC has only antibonding orbitals with the neighboring layers. The latter causes states close to the Fermi level to have a larger weight in the outer layers and on atoms with no vertically close neighbors. In Fig. 1a, we show a side view of the unit cell of the ABC trilayer and the location of the states from $E_F - 0.5$ eV to E_F obtained from a DFT calculation of an ABC trilayer under an external electric field to separate valence and conduction bands. As can be seen, they are located in the B_1 and B_3 atoms of the outer layers, which have no vertical neighbors in the middle layer. Nonetheless, in both cases, we observe flat bands a few meV away from the Fermi level. These states would be related to the collective phenomena observed in several experiments [22,23,25].

3.2. Two rotated ABC trilayers

In systems with few atomic layers, the environment of each atomic sheet modifies the electronic structure. This can be understood as a two-dimensional analogue of the crystal field that appears in some three-dimensional materials [53,54]. We previously found that the asymmetry between layers caused gap opening [27,28]; here we show that a similar behavior occurs in two ABC trilayers with a rotation angle between them.

Fig. 2 illustrates DFT calculations of band structures for four rotation angles (21.8°, 13.4°, 9.4°, and 6.0°). The system of two trilayers ABC coupled with a rotation angle between them (2ABCT) has a gap, even though each ABC trilayer does not. The bandgap is around 30 meV, and its origin is similar to DTBG or even of a trilayer ABA [55]. The different environments of the layers, and hence their couplings, cause a gap opening due to symmetry. When the two ABC structures are coupled, the inversion symmetry that preserves the sublayer exchange symmetry of each ABC structure is broken, opening the gap. The differences in the interlayer couplings to adjacent layers can be modeled as the application of different potentials in each layer: Therefore, charge transfers between their are expected to occur.

This assertion is corroborated by calculations of the charge density distribution over the whole supercell including all states of the system below the Fermi level, differently from that shown in Fig. 1a, where only states near the Fermi level are considered. We then subtract the contribution of each layer separately; in total, seven calculations were performed, one for the whole structure and six self-consistent calculations without relaxation for each layer. We consider the value of the charge in each layer as the sum of the average charge between $-c/2$ and $+c/2$ from the layer position (c is the average distance between layers). According to the analysis, the middle layers lose charge, whereas the second and fifth layers receive most of the charge. We analyzed different rotational angles ($n = 2, 3$ and 4) with similar results.

It is important to notice that a TB Hamiltonian only allows us to obtain the gap if we add an onsite energy term in each layer.

Let us now analyze the spatial localization of states from the flat band region near the Fermi level in rotated structures. Fig. 3 shows the localization of states near the K point, both in the two highest valence bands (a) and in the lowest conduction bands (b), obtained with the DFT method. The states in the valence band are spatially localized mostly in the intermediate layers, i.e., the rotated layers. For this angle (9.4°), there is still no clear localization in the AA sites, although the moiré pattern begins to be visualized. An inset of Fig. 3a bottom panel

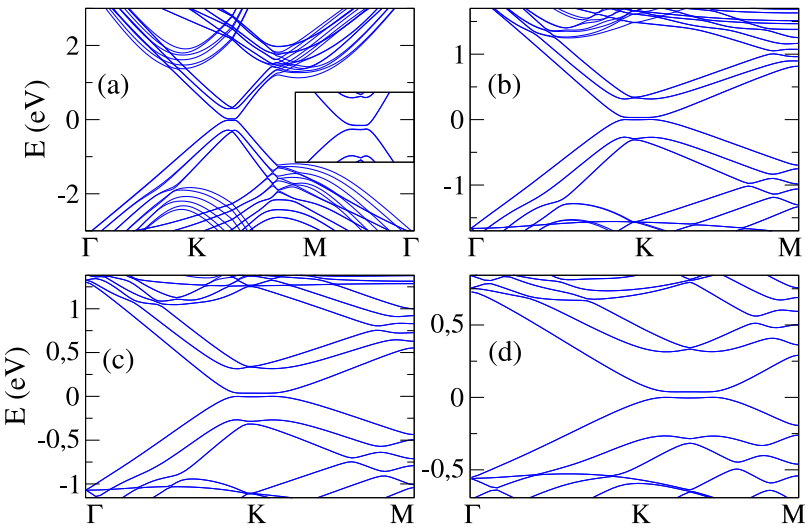

Fig. 2. DFT calculations of the band structure of double ABC trilayer twisted for four different angles (a) $\theta = 21.8°$ (b) $\theta = 13.1°$ (c) $\theta = 9.4°$ (d) $\theta = 6.0°$.

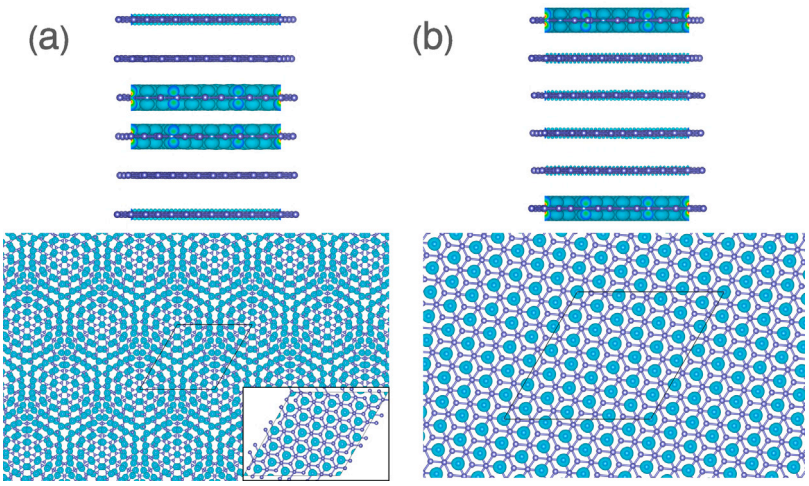

Fig. 3. DFT calculations of side and top views of localization of states around the K point for (a) the two highest occupied valence bands(layers 3 and 4 are shown in the bottom panel, and in the inset layers 4 and 5), (b) the two lowest conduction bands. In the bottom panel, only layers 5 and 6 are shown. The rotational angle between layers is 9.4°.

reveals that the states are localized in the bonding orbitals, i.e., in an atom in the center of the hexagon of the neighboring Bernal layer, as it also occurs in trilayer ABC. If we electrostatically doped the system, we would find that the states are now essentially in the outer layers and, likewise, in the B-type atoms (Fig. 3b).

3.3. Electronic localization for low angles

The localization of electrons in the AA region of the unit cell is the hallmark of rotated bilayer graphene; this is one of the reasons electronic correlations occur since most part of the charge associated with the two highest valence bands is located in this region [56].

To analyze how the localization evolves for smaller angles, we use the TB Hamiltonian. In Appendix B we show the band structure for six rotated structures calculated with the TB model.

We compute the projection of the states of the two highest valence bands (HVB) on each layer as follows:

$$n_l = \sum_{j \in L_l} \frac{1}{N_k} \sum_{n \in HVB} \sum_{k} |\langle \Psi_{nk} | \phi_j \rangle|^2 , \tag{5}$$

where Ψ_{nk} is the wavefunction of the system for an eigenvalue n at a given k point, ϕ_j is the orbital at site j. Note that the sum over n comprises only states in the two HVB, the sum over k represents the integration over the Brillouin zone, and the sum over j includes all the orbitals in layer l. This magnitude multiplied by the electron charge [57] quantifies the charge distribution associated with each layer of the above-mentioned bands. In the following, we will call it simply charge.

Fig. 4a shows how the charge n_l of the two HVB evolves as a function of the angle. Due to symmetry, the pair of layers 1–6, 2–5, and 3–4 have the same charge. Layers 3–4 are rotated with respect to each other; initially, as the angle decreases, the localization in these layers increases. However, contrary to what happens in the TBG for angles below 2.5°, the charge drastically starts to escape from these layers, moving to layer 1.

4. Discussion

To understand why the charge escapes from twisted layers, we analyze a simpler trilayer ABA graphene system with a twisted third layer; we will denote this system as ABT. Fig. 4b shows that the redistribution of charge within layers is similar to the 2ABCT. In Appendix C we show how that charge is redistributed within the three layers of an ABT system for a rotational angle of 1.3°.

If we break down how the charge redistributes by sublattice in layer 1, we see that it goes to the B-type bonding atoms (see Figs. 1 and 4d).

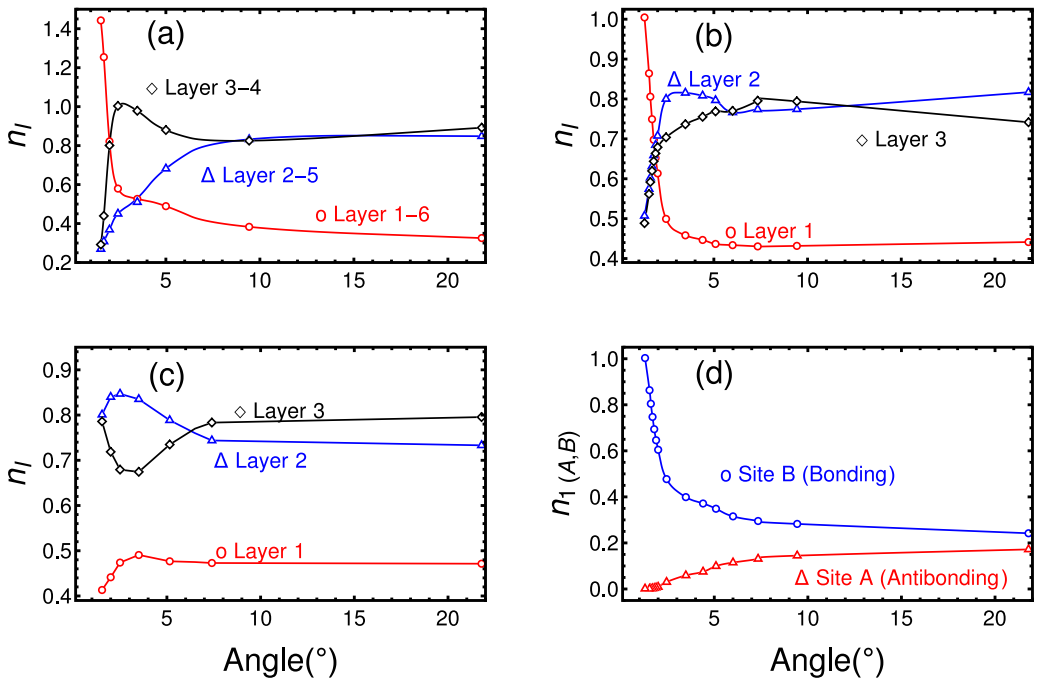

Fig. 4. Charge as defined in Eq. (5) for each layer as a function of the angle for (a) double-twisted trilayer ABC, (b) trilayer ABT, (c) trilayer ABT with a negative external electric field. (d) n_l projected on sublattices A and B on layer 1 of trilayer ABT.

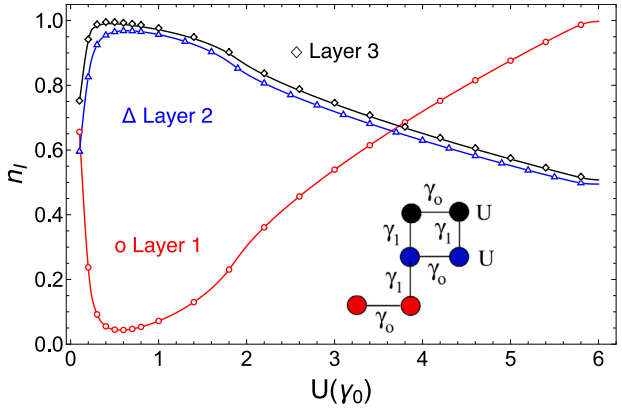

Fig. 5. Charge redistribution as a function of U in each layer of a toy model: Three graphene layers with stacking ABB, with an onsite energy U on layers 2–3. In the scheme, γ_o and γ_1 are intra- and interlayer hoppings of graphene.

The latter is not surprising; it is similar to what happens in the Bernal bilayer or trilayer ABC; the highest valence states prefer to be in the bonding type atoms of layer 1. However, it is different in ABT because we have two competing variables: the moiré potential and the coupling with the first layer.

Let us rationalize why the charge moves to layer 1. In TBG the periodic moiré potential confines electrons in the AA zones of the rotated layers; adding an extra layer provides an extra coupling and an additional region to which the electron can move. A simplified way to understand this is to think that the energy of an electron in the AA region increases due to Coulomb repulsion, so it moves to another place to lower the repulsion and the total energy. In this case, these are B-type atoms of layer 1.

However, using a toy model, we explain the previous results. Let us take a structure with ABB stacking, with the typical intra- (γ_0) and interlayer (γ_1) hoppings of graphene, and put an onsite potential U in layers 2–3 (with BB stacking). In this way, we simulate an increase in the electron energy in those layers. An increase of U would be equivalent to a decrease of the rotation angle. The inset of Fig. 5 schematically depicts the model. We calculate the charge associated with the last two valence bands and plot n_l as a function of U. Initially, the charge is higher in the BB layers (2 and 3), but for U larger than $\sim \gamma_0/2$ there is a reversal of this trend, as it can be seen in Fig. 5. The charge accumulates more in layer 1 for large values of U. This is precisely the behavior of the rotated trilayer ABT.

Notice that in our toy model, values up to $U = 6\gamma_0$ have been chosen in order to have a Coulomb energy comparable to the bandwidth, which is several times γ_0, so that the potential energy is comparable to the kinetic energy of the relevant band.

This phenomenon does not occur in DTBG or three-layer graphene (ATA), in which the middle layer is twisted. Incidentally, a superconducting phase has been found in these two systems, while only a Mott insulating phase has been found in ABT [58,59].

A negative external electric field preserves the localization in the upper layers [59]. In Fig. 4d, we show the charge localization in trilayer ABT under an external negative electric field $\mathbf{E} = 20$ meV/Å $\hat{z}$. However, it does not reach the level of localization observed in TBG [56], this can be explained by looking at the band structure: The field does not reduce the bandwidth and, therefore, the kinetic energy of the electrons in those bands. See Appendix D for more information.

5. Summary and conclusions

In summary, we study the electron localization in a system composed of two ABC trilayers (six layers in total) rotated to each other. The system is semiconducting for large angles; the gap opens spontaneously due to the crystal field. The localization in the layers is similar to that found in an ABC trilayer subjected to a small external field. However, for small angles of rotation (less than 2°), the localization does not follow the same trend as in TBG, where electrons concentrate in the AA region of the unit cell; in this system, the electrons leak to the outer layers. We argue that this is due to the presence of an extra coupled layer that allows the electrons to move to lower energy levels/states as the energy of the electrons increases due to the enhanced Coulomb interaction. This behavior resembles an ABT system

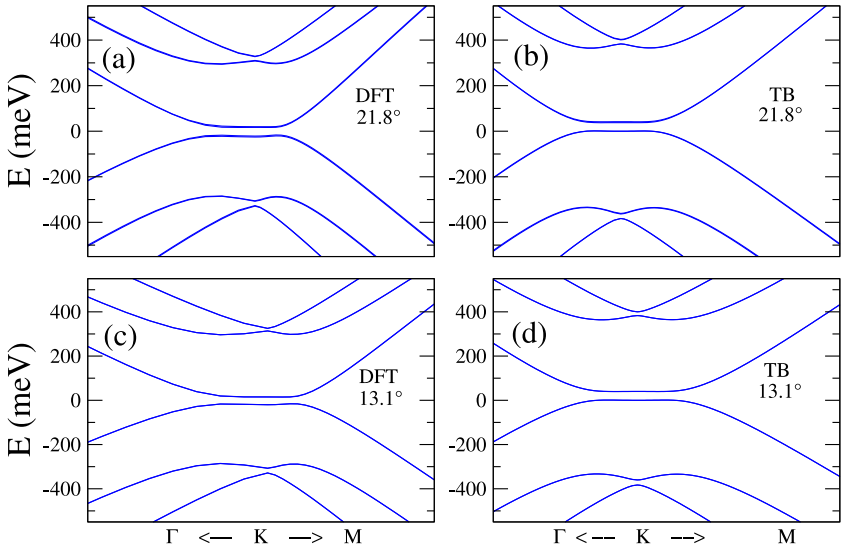

Fig. A.1. A comparison of DFT (left panels) and TB (right panels) calculated bands around the K point. The top rows for a relative rotation angle $\theta = 21.8°$ and the bottom rows for $\theta = 13.1°$.

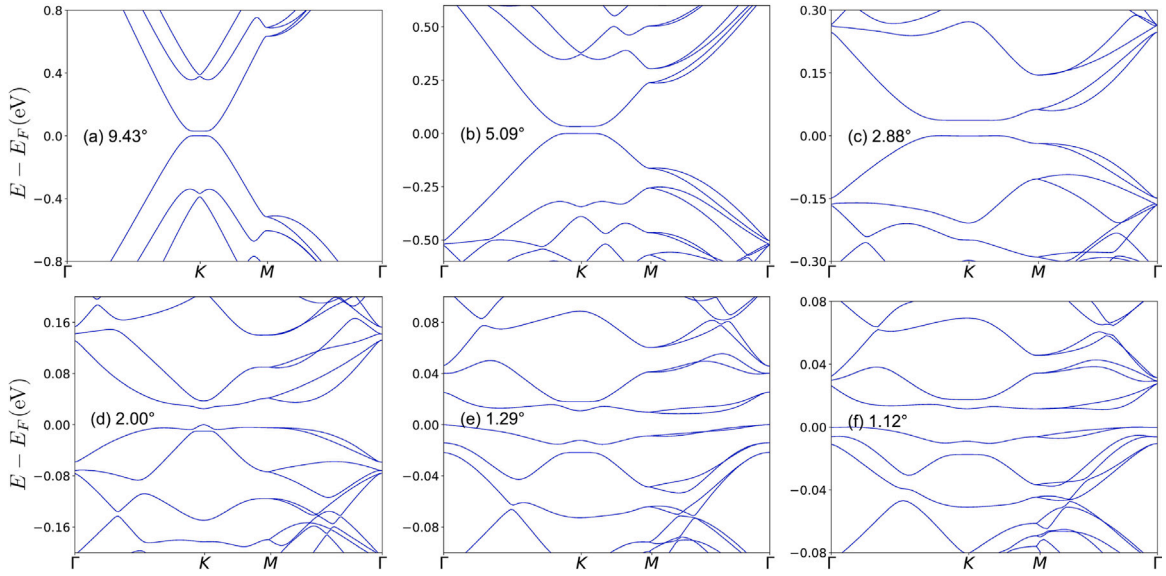

Fig. B.1. Band structure of double trilayer ABC twisted for six rotational angles (a) 9.43° (b) 5.09° (c) 2.88° (d) 2.00° (e) 1.20° (f) 1.12°.

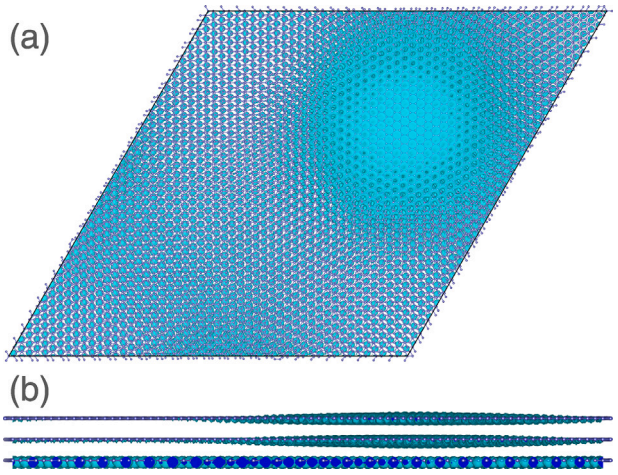

Fig. C.1. Localization of charge associated with the two highest valence bands in trilayer ABT for a rotational angle of 1.3° (a) top view (b) lateral view.

(three layers with ABA stacking and the last layer rotated). A negative electric field prevents the charge from spilling from the rotated layers.

Finally, we show that the charge leakage out of the rotated layers is associated with an increase in the energy of the electrons in those layers due to Coulomb interaction. Using a toy model, we reveal that by increasing the energy of specific layers, the charge follows the same behavior as that found in structures based on rotated graphene trilayers. The charge leakage to outer layers due to Coulomb repulsion explains the gap opening in such structures and the depletion of the high-density AA zones for small twist angles. It provides a rationale for the absence of superconductivity in these trilayer-based systems.

CRediT authorship contribution statement

Felipe Pérez Riffo: Software, Investigation. **Sanber Vizcaya:** Software, Investigation. **E. Menéndez-Proupin:** Writing – original draft, Methodology, Investigation. **Juan M. Florez:** Writing – review & editing, Investigation. **Leonor Chico:** Writing – original draft, Conceptualization. **Eric Suárez Morell:** Writing – original draft, Methodology, Conceptualization.

Declaration of competing interest

The authors declare that they have no known competing financial interests or personal relationships that could have appeared to influence the work reported in this paper.

Acknowledgments

ESM and JMF acknowledge financial support from FONDECYT Regular 1221301 (Chile) and María Zambrano Program, Ministry of Universities, and Seville University, Spain. LC acknowledges financial support from the Spanish Ministry of Science and Innovation (grant PID2022-136285NB-C31) and the "(MAD2D-CM)-(UCM5)" project funded by Comunidad de Madrid, Spain, by the Recovery, Transformation and Resilience Plan, and by NextGenerationEU from the European Union. Powered@NLHPC: This research was partially supported by the supercomputing infrastructure of the NLHPC (ECM-02).

Appendix A. Comparison of DFT and TB calculations

In Fig. A.1, we compare the electronic structure at low energies of the DFT and TB calculations for angles 13.1° and 21.7°. The agreement is excellent. Note that the system is a semiconductor, and the bands are flat near the Fermi level.

Appendix B. TB calculations

Fig. B.1 shows the calculations with the TB model of double trilayer ABC twisted for six rotational angles. All calculations were done with the previously relaxed unit cells.

All six structures are semiconducting.

Appendix C. Charge localization for low angles

In Fig. C.1 we show a calculation of the charge localizations as defined in Eq. (5) of the main text. In the top panel, it can be seen that the charge associated with the two HVBs is localized in the AA region; however, in the lateral view, it is clear that there is also a dispersed charge in the first layer.

Furthermore, as we showed in the main part, the charge in the first layer is mainly localized in atoms of sublattice B, the bonding ones.

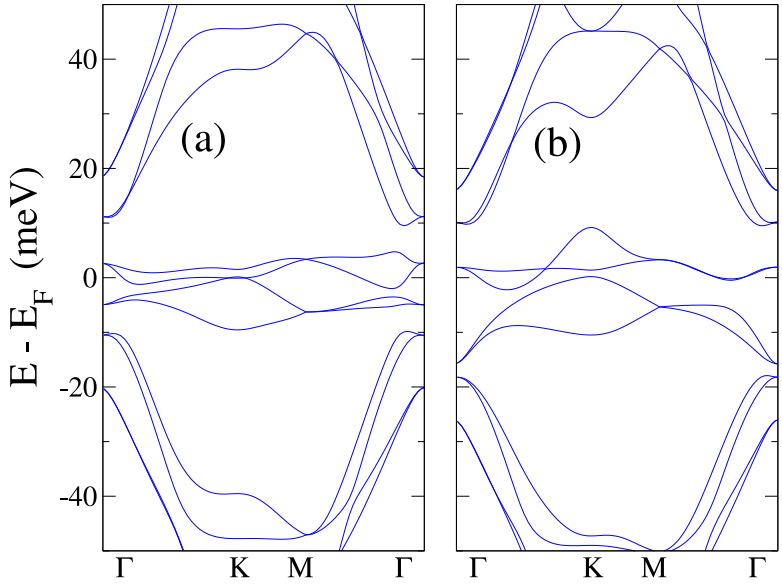

Fig. D.1. Band structure of trilayer ABT for a rotational angle of 1.05° (a) without and (b) with an external electric field of **E** = −80 meV/Å.

Appendix D. Trilayer ABT under an electric field

As shown in the main text, a negative external field prevents the leakage of charge from the rotated layers. However, in the band structure (Fig. D.1), the field does not reduce the bandwidth and, therefore, the kinetic energy of the electrons in those bands. The electrons would not be as localized as in the TBG.

The field's value is the same as we use in the main text to calculate the charge redistribution within layers. The system is metallic with no external field and remains so for relatively small fields, but for larger ones, it becomes semiconducting.

References

[1] J.M.B. Lopes dos Santos, N.M.R. Peres, A.H. Castro Neto, Graphene bilayer with a twist: Electronic structure, Phys. Rev. Lett. 99 (2007) 256802, http://dx.doi.org/10.1103/PhysRevLett.99.256802.

[2] E. Suárez Morell, J.D. Correa, P. Vargas, M. Pacheco, Z. Barticevic, Flat bands in slightly twisted bilayer graphene: Tight-binding calculations, Phys. Rev. B 82 (2010) 121407, http://dx.doi.org/10.1103/PhysRevB.82.121407.

[3] G. Trambly de Laissardière, D. Mayou, L. Magaud, Localization of dirac electrons in rotated graphene bilayers, Nano Lett. 10 (2010) 804–808, http://dx.doi.org/10.1021/nl902948m.

[4] G. Li, A. Luican, J.M.B. Lopes dos Santos, A.H. Castro Neto, A. Reina, J. Kong, E.Y. Andrei, Observation of Van Hove singularities in twisted graphene layers, Nat. Phys. 6 (2009) 109–113, http://dx.doi.org/10.1038/nphys1463.

[5] R. Bistritzer, A.H. MacDonald, Moiré bands in twisted double-layer graphene, Proc. Natl. Acad. Sci. 108 (2011) 12233–12237, http://dx.doi.org/10.1073/pnas.1108174108.

[6] E. Suárez Morell, P. Vargas, L. Chico, L. Brey, Charge redistribution and interlayer coupling in twisted bilayer graphene under electric fields, Phys. Rev. B 84 (2011) 195421, http://dx.doi.org/10.1103/PhysRevB.84.195421.

[7] Y. Cao, V. Fatemi, S. Fang, K. Watanabe, T. Taniguchi, E. Kaxiras, P. Jarillo-Herrero, Unconventional superconductivity in magic-angle graphene superlattices, Nature 556 (2018) 43–50, http://dx.doi.org/10.1038/nature26160.

[8] J.M. Park, Y. Cao, K. Watanabe, T. Taniguchi, P. Jarillo-Herrero, Tunable strongly coupled superconductivity in magic-angle twisted trilayer graphene, Nature 590 (7845) (2021) 249–255, http://dx.doi.org/10.1038/s41586-021-03192-0.

[9] Y. Cao, D. Rodan-Legrain, O. Rubies-Bigorda, J.M. Park, K. Watanabe, T. Taniguchi, P. Jarillo-Herrero, Tunable correlated states and spin-polarized phases in twisted bilayer–bilayer graphene, Nature 583 (7815) (2020) 215–220, http://dx.doi.org/10.1038/s41586-020-2260-6.

[10] O. Arroyo-Gascón, R. Fernández-Perea, E.S. Morell, C. Cabrillo, L. Chico, Universality of moiré physics in collapsed chiral carbon nanotubes, Carbon 205 (2023) 394–401, http://dx.doi.org/10.1016/j.carbon.2023.01.052.

[11] O. Arroyo-Gascón, R. Fernández-Perea, E.S. Morell, C. Cabrillo, L. Chico, One-dimensional moiré superlattices and flat bands in collapsed chiral carbon nanotubes, Nano Lett. 20 (10) (2020) 7588–7593, http://dx.doi.org/10.1021/acs.nanolett.0c03091.

[12] A.H. Castro Neto, F. Guinea, N.M.R. Peres, K.S. Novoselov, A.K. Geim, The electronic properties of graphene, Rev. Modern Phys. 81 (2009) 109–162, http://dx.doi.org/10.1103/RevModPhys.81.109, URL http://link.aps.org/doi/10.1103/RevModPhys.81.109.

[13] F. Guinea, A.H. Castro Neto, N.M.R. Peres, Electronic states and landau levels in graphene stacks, Phys. Rev. B 73 (2006) 245426, http://dx.doi.org/10.1103/PhysRevB.73.245426, URL http://link.aps.org/doi/10.1103/PhysRevB.73.245426.

[14] B. Partoens, F.M. Peeters, From graphene to graphite: Electronic structure around the k point, Phys. Rev. B 74 (2006) 075404, http://dx.doi.org/10.1103/PhysRevB.74.075404, URL http://link.aps.org/doi/10.1103/PhysRevB.74.075404.

[15] F. Zhang, B. Sahu, H. Min, A.H. MacDonald, Band structure of *abc*-stacked graphene trilayers, Phys. Rev. B 82 (2010) 035409, http://dx.doi.org/10.1103/PhysRevB.82.035409, URL http://link.aps.org/doi/10.1103/PhysRevB.82.035409.

[16] M. Aoki, H. Amawashi, Dependence of band structures on stacking and field in layered graphene, Solid State Commun. 142 (3) (2007) 123–127, http://dx.doi.org/10.1016/j.ssc.2007.02.013, URL http://www.sciencedirect.com/science/article/pii/S0038109807001184.

[17] Y.-P. Lin, J. Wang, J.-M. Lu, C.-Y. Lin, M.-F. Lin, Energy spectra of abc-stacked trilayer graphene in magnetic and electric fields, RSC Adv. 4 (2014) 56552–56560, http://dx.doi.org/10.1039/C4RA10860D.

[18] S.H. Jhang, M.F. Craciun, S. Schmidmeier, S. Tokumitsu, S. Russo, M. Yamamoto, Y. Skourski, J. Wosnitza, S. Tarucha, J. Eroms, C. Strunk, Stacking-order dependent transport properties of trilayer graphene, Phys. Rev. B 84 (2011) 161408, http://dx.doi.org/10.1103/PhysRevB.84.161408, URL http://link.aps.org/doi/10.1103/PhysRevB.84.161408.

[19] H. Wang, J.-H. Gao, F.-C. Zhang, Flat band electrons and interactions in rhombohedral trilayer graphene, Phys. Rev. B 87 (2013) 155116, http://dx.doi.org/10.1103/PhysRevB.87.155116, URL http://link.aps.org/doi/10.1103/PhysRevB.87.155116.

[20] C.H. Lui, Z. Li, K.F. Mak, E. Cappelluti, T.F. Heinz, Observation of an electrically tunable band gap in trilayer graphene, Nat. Phys. 7 (12) (2011) 944–947, http://dx.doi.org/10.1038/nphys2102.

[21] T. Khodkov, I. Khrapach, M.F. Craciun, S. Russo, Direct observation of a gate tunable band gap in electrical transport in abc-trilayer graphene, Nano Lett. 15 (7) (2015) 4429–4433, arXiv:https://doi.org/10.1021/acs.nanolett.5b00772.

[22] H. Zhou, T. Xie, A. Ghazaryan, T. Holder, J.R. Ehrets, E.M. Spanton, T. Taniguchi, K. Watanabe, E. Berg, M. Serbyn, A.F. Young, Half- and quarter-metals in rhombohedral trilayer graphene, Nature 598 (7881) (2021) 429, http://dx.doi.org/10.1038/s41586-021-03938-w.

[23] H. Zhou, T. Xie, T. Taniguchi, K. Watanabe, A.F. Young, Superconductivity in rhombohedral trilayer graphene, Nature 598 (7881) (2021) 434, http://dx.doi.org/10.1038/s41586-021-03926-0.

[24] G. Chen, L. Jiang, S. Wu, B. Lyu, H. Li, B.L. Chittari, K. Watanabe, T. Taniguchi, Z. Shi, J. Jung, Y. Zhang, F. Wang, Evidence of a gate-tunable mott insulator in a trilayer graphene moiré superlattice, Nat. Phys. 15 (3) (2019) 237–241, http://dx.doi.org/10.1038/s41567-018-0387-2.

[25] S. Lee, J. Che, Y. Velasco Jr., Y. Gao, D. Shi, J. Tran, F. Baima, M. Mauri, M. Calandra, C.N. Bockrath, X. Lau, Gate-tunable magnetism and giant magnetoresistance in suspended rhombohedral-stacked few-layer graphene, Nano Lett. 22 (13) (2022) 5094–5099, http://dx.doi.org/10.1021/acs.nanolett.2c00466.

[26] P.A. Pantaleón, A. Jimeno-Pozo, H. Sainz-Cruz, V.T. Phong, T. Cea, F. Guinea, Superconductivity and correlated phases in non-twisted bilayer and trilayer graphene, Nat. Rev. Phys. 5 (5) (2023) 304–315, http://dx.doi.org/10.1038/s42254-023-00575-2.

[27] E. Suárez Morell, M. Pacheco, L. Chico, L. Brey, Electronic properties of twisted trilayer graphene, Phys. Rev. B 87 (2013) 125414, http://dx.doi.org/10.1103/PhysRevB.87.125414, URL http://link.aps.org/doi/10.1103/PhysRevB.87.125414.

[28] F.J. Culchac, R.R. Del Grande, R.B. Capaz, L. Chico, E.S. Morell, Flat bands and gaps in twisted double bilayer graphene, Nanoscale 12 (2020) 5014–5020, http://dx.doi.org/10.1039/C9NR10830K.

[29] M. Koshino, Band structure and topological properties of twisted double bilayer graphene, Phys. Rev. B 99 (2019) 235406, http://dx.doi.org/10.1103/PhysRevB.99.235406, URL http://link.aps.org/doi/10.1103/PhysRevB.99.235406.

[30] Y.W. Choi, H.J. Choi, Intrinsic band gap and electrically tunable flat bands in twisted double bilayer graphene, Phys. Rev. B 100 (2019) 201402, http://dx.doi.org/10.1103/PhysRevB.100.201402, URL http://link.aps.org/doi/10.1103/PhysRevB.100.201402.

[31] P. Rickhaus, G. Zheng, J.L. Lado, Y. Lee, A. Kurzmann, M. Eich, R. Pisoni, C. Tong, R. Garreis, C. Gold, M. Masseroni, T. Taniguchi, K. Watanabe, T. Ihn, K. Ensslin, Gap opening in twisted double bilayer graphene by crystal fields, Nano Lett. 19 (12) (2019) 8821–8828, http://dx.doi.org/10.1021/acs.nanolett.9b03660.

[32] C. Shen, Y. Chu, Q. Wu, N. Li, S. Wang, Y. Zhao, J. Tang, J. Liu, J. Tian, K. Watanabe, T. Taniguchi, R. Yang, Z.Y. Meng, D. Shi, O.V. Yazyev, G. Zhang, Correlated states in twisted double bilayer graphene, Nat. Phys. 16 (5) (2020) 520–525, http://dx.doi.org/10.1038/s41567-020-0825-9.

[33] M. Cohen, Chapter 1 overview: A standard model of solids, in: S.G. Louie, M.L. Cohen (Eds.), Conceptual Foundations of Materials, in: Contemporary Concepts of Condensed Matter Science, vol. 2, Elsevier, 2006, pp. 1–8, http://dx.doi.org/10.1016/S1572-0934(06)02001-4, URL http://www.sciencedirect.com/science/article/pii/S1572093406020014.

[34] S. Louie, Chapter 2 predicting materials and properties: Theory of the ground and excited state, in: S.G. Louie, M.L. Cohen (Eds.), Conceptual Foundations of Materials, in: Contemporary Concepts of Condensed Matter Science, vol. 2, Elsevier, 2006, pp. 9–53, http://dx.doi.org/10.1016/S1572-0934(06)02002-6, URL http://www.sciencedirect.com/science/article/pii/S1572093406020026.

[35] B. Pahlevanzadeh, P. Sahebsara, D. Sénéchal, Chiral p-wave superconductivity in twisted bilayer graphene from dynamical mean field theory, SciPost Phys. 11 (2021) 017, http://dx.doi.org/10.21468/SciPostPhys.11.1.017, URL http://scipost.org/10.21468/SciPostPhys.11.1.017.

[36] J.S. Hofmann, E. Khalaf, A. Vishwanath, E. Berg, J.Y. Lee, Fermionic monte carlo study of a realistic model of twisted bilayer graphene, Phys. Rev. X 12 (2022) 011061, http://dx.doi.org/10.1103/PhysRevX.12.011061, URL http://link.aps.org/doi/10.1103/PhysRevX.12.011061.

[37] Python code to generate Unit cell(https://esmorell.cl/codes/).

[38] H.T. Stokes, D.M. Hatch, Findsym: program for identifying the space-group symmetry of a crystal, J. Appl. Cryst. 38 (1) (2005) 237–238, http://dx.doi.org/10.1107/s0021889804031528.

[39] P.E. Blöchl, Projector augmented-wave method, Phys. Rev. B 50 (1994) 17953–17979.

[40] G. Kresse, D. Joubert, From ultrasoft pseudopotentials to the projector augmented wave method, Phys. Rev. B 59 (1999) 1758–1775.

[41] G. Kresse, J. Furthmüller, Efficiency of ab-initio total energy calculations for metals and semiconductors using a plane-wave basis set, Comput. Mater. Sci. 6 (1996) 15.

[42] G. Kresse, J. Furthmüller, Efficient iterative schemes for ab initio total-energy calculations using a plane-wave basis set, Phys. Rev. B 54 (1996) 11169–11186.
[43] J.P. Perdew, K. Burke, M. Ernzerhof, Generalized gradient approximation made simple, Phys. Rev. Lett. 77 (1996) 3865–3868.
[44] S. Grimme, J. Antony, S. Ehrlich, H. Krieg, A consistent and accurate ab initio parametrization of density functional dispersion correction (DFT-D) for the 94 elements H-Pu, J. Chem. Phys. 132 (15) (2010) 154104, arXiv:https://doi.org/10.1063/1.3382344.
[45] S. Grimme, S. Ehrlich, L. Goerigk, Effect of the damping function in dispersion corrected density functional theory, J. Comput. Chem. 32 (2011) 1456–1465, arXiv:https://onlinelibrary.wiley.com/doi/pdf/10.1002/jcc.21759 URL http://onlinelibrary.wiley.com/doi/abs/10.1002/jcc.21759.
[46] N.N.T. Nam, M. Koshino, Lattice relaxation and energy band modulation in twisted bilayer graphene, Phys. Rev. B 96 (7) (2017) 075311, http://dx.doi.org/10.1103/PhysRevB.96.075311.
[47] S. Plimpton, Fast parallel algorithms for short-range molecular dynamics, J. Comput. Phys. 117 (1995) 1, http://dx.doi.org/10.1006/jcph.1995.1039.
[48] A.N. Kolmogorov, V.H. Crespi, Registry-dependent interlayer potential for graphitic systems, Phys. Rev. B 71 (2005) 235415, http://dx.doi.org/10.1103/PhysRevB.71.235415.
[49] W. Ouyang, D. Mandelli, M. Urbakh, O. Hod, Nanoserpents: Graphene nanoribbon motion on two-dimensional hexagonal materials, Nano Lett. 18 (2018) 6009–6016, http://dx.doi.org/10.1021/acs.nanolett.8b02848.
[50] D. Brenner, S.O. A, J.A. Harrison, S.J. Stuart, B. Ni, S.S. B, A second-generation reactive empirical bond order (rebo) potential energy expression for hydrocarbons, J. Phys. - Condens. Matter 14 (2003) 783, http://dx.doi.org/10.1088/0953-8984/14/4/312.
[51] S. Stuart, A.B. Tutein, J.A. Harrison, A reactive potential for hydrocarbons with intermolecular interactions, J. Chem. Phys. 112 (2000) 6472, http://dx.doi.org/10.1063/1.481208.
[52] X. Liang, Z.A.H. Goodwin, V. Vitale, F. Corsetti, A.A. Mostofi, J. Lischner, Effect of bilayer stacking on the atomic and electronic structure of twisted double bilayer graphene, Phys. Rev. B 102 (2020) 155146, http://dx.doi.org/10.1103/PhysRevB.102.155146, URL http://link.aps.org/doi/10.1103/PhysRevB.102.155146.
[53] H. Bethe, Termaufspaltung in kristallen, Ann. Phys. 395 (2) (1929) 133–208, http://dx.doi.org/10.1002/andp.19293950202.
[54] J.H.V. Vleck, Theory of the variations in paramagnetic anisotropy among different salts of the iron group, Phys. Rev. 41 (2) (1932) 208–215, http://dx.doi.org/10.1103/physrev.41.208.
[55] M.G. Menezes, R.B. Capaz, S.G. Louie, Ab initio quasiparticle band structure of aba and abc-stacked graphene trilayers, Phys. Rev. B 89 (2014) 035431, http://dx.doi.org/10.1103/PhysRevB.89.035431, URL http://link.aps.org/doi/10.1103/PhysRevB.89.035431.
[56] G. Trambly de Laissardière, D. Mayou, L. Magaud, Numerical studies of confined states in rotated bilayers of graphene, Phys. Rev. B 86 (2012) 125413, http://dx.doi.org/10.1103/PhysRevB.86.125413, URL http://link.aps.org/doi/10.1103/PhysRevB.86.125413.
[57] R.A. Millikan, On the elementary electrical charge and the avogadro constant, Phys. Rev. 2 (1913) 109–143, http://dx.doi.org/10.1103/PhysRev.2.109, URL http://link.aps.org/doi/10.1103/PhysRev.2.109.
[58] S. Chen, M. He, Y.-H. Zhang, V. Hsieh, Z. Fei, K. Watanabe, T. Taniguchi, D.H. Cobden, X. Xu, C.R. Dean, M. Yankowitz, Electrically tunable correlated and topological states in twisted monolayer–bilayer graphene, Nat. Phys. 17 (3) (2021) 374–380, http://dx.doi.org/10.1038/s41567-020-01062-6.
[59] S.-y. Li, Z. Wang, Y. Xue, Y. Wang, S. Zhang, J. Liu, Z. Zhu, K. Watanabe, T. Taniguchi, H.-j. Gao, Y. Jiang, J. Mao, Imaging topological and correlated insulating states in twisted monolayer-bilayer graphene, Nature Commun. 13 (1) (2022) 4225, http://dx.doi.org/10.1038/s41467-022-31851-x.